A FINITE VOLUME METHOD FOR TRANSONIC POTENTIAL FLOW CALCULATIONS[*]

A. Jameson   D. A. Caughey

Abstract

It is proposed to solve the exact transonic potential flow equation on a mesh constructed from small volume elements, which can be conveniently packed around any reasonably smooth configuration. the calculation is performed on two sets of interlocking cells. The velocity and density are calculated in the primary cells, and a flux balance is then established in the secondary cells. The scheme is desymmetrized by the addition of artificial viscosity in the supersonic zone. Some results are included for a swept wing and a wing-cylinder combination.

1   Introduction

The purpose of this paper is to propose a method for calculating transonic potential flows which can be applied to bodies of more or less arbitrary geometric complexity, given a sufficiently powerful computer. Following the success of Murman and Cole[1,2] in obtaining numerical solutions of the transonic small disturbance equation, relaxation methods have been used to solve both the transonic small disturbance and the exact potential flow equations for a variety of special configurations.[3−6] A major difficulty in solving the exact potential flow equation lies in the construction of sufficiently accurate discrete approximations to the boundary conditions.

It is proposed here to circumvent the geometric difficulties by deriving a discrete approximation on a mesh constructed from small volume elements which can be conveniently packed around the body. This leads to a relatively simple treatment of the exact potential flow equation in conservation form. In its motivation the scheme is comparable to the finite volume method proposed by

MacCormack and Rizzi[7,8] to treat the Euler equations and other first order hyperbolic systems of equations. Since, however, the potential flow equation is of second order, the new scheme is constructed using two sets of interlocking cells, a primary set in which the velocity and density are calculated from the potential, and a secondary set in which a flux balance is established.

The scheme can be regarded as a finite element method, adapted to treat regions of locally supersonic flow by the addition of an artificial viscosity. The basic formulas in regions of locally subsonic flow could in fact be derived from the Bateman variational principal.[9] Another way to derive these formulas is to apply the box scheme twice, first in the primary cells and then in the secondary cells. Thus the scheme for the two sets of cells can also be regarded as a staggered box scheme, in which difference formulas are used to evaluate transformation coefficients defining local mappings of each primary box in the computational domain to a volume element in the physical domain.

2   Formulation

It will be assumed that any shock waves contained in the flows to be computed are weak enough that the entropy and vorticity generated by the shock waves can be ignored without introducing serious errors. Consistent with this approximation we shall treat the exact potential flow equation in conservation form. Using Cartesian coordinates x, y, z we shall write this equation as

$$\frac{\partial}{\partial x}(\rho u) + \frac{\partial}{\partial y}(\rho v) + \frac{\partial}{\partial z}(\rho w) = 0 \tag{1}$$

where ρ is the density and u, v, w are the velocity components. These are calculated as the gradient of the potential Φ.

$$u = \Phi_x, \quad v = \Phi_y, \quad w = \phi_z. \tag{2}$$

The flow is assumed to be uniform in the far field with a Mach number M_∞. At the body, the boundary condition is

$$u_n = 0 \tag{3}$$

where u_n is the normal velocity component. The density is computed from the isentropic formula.

$$\rho = \{1 + \frac{\gamma - 1}{2}M_\infty^2(1 - q^2)\}^{\frac{1}{\gamma-1}} \tag{4}$$

where ρ is the ratio of specific heats, and q is the speed,

$$q^2 = u^2 + v^2 + w^2 \tag{5}$$

With the normalization that $q = 1$ and $p = 1$ at infinity, the corresponding formulas for the pressure p and the local speed of

$$p = \frac{\rho^\gamma}{\gamma M_\infty^2}, \quad a^2 = \frac{\rho^{\gamma-1}}{M_\infty^2}. \tag{6}$$

The shock jump conditions are

(a) continuity of Φ, implying a continuity of the tangential velocity component;

(b) continuity of ρu_n, where u_n is the normal velocity component.

Under the isentropic assumption the normal component of momentum is not conserved through the shock wave, leading to a body force which is an approximation to the wave drag. In any finite domain equations $(1) - (5)$ together with the shock jump relations (a) and (b) are equivalent to the Bateman variational principle that the integral

$$I = \int_\Omega p \, d\Omega \tag{7}$$

is stationary.

A difficulty with the formulation assuming potential flow is that corresponding to any solution of equation (1) there is a reverse flow solution, in which compression shock waves become expansion shock waves. In fact if central difference formulas are used throughout the domain, symmetric solutions, containing an expansion shock at the front and a compression shock at the rear, can be computed for a body with fore and aft symmetry such as an ellipse. This is a consequence of the absence of entropy from the formulation. In order to obtain a unique and physically relevant solution the shock jump relations (a) and (b) must be supplemented by the additional "entropy condition" that discontinuous expansions are to be excluded from the solution, corresponding to the fact that entropy cannot decrease in a real flow.

For this purpose the discrete approximation will be desymmetrized by the addition of artificial viscosity to produce an upwind bias in the supersonic zone. The added terms will be introduced in a manner such that the conservation form of equation (1) is preserved. Provided that the solution of the discrete equations converges in the limit as the cell width is reduced to zero, the correct shock jump relations consistent with the isentropic assumption will then be a natural consequence of the scheme.[10]

3 The Staggered Box Scheme

The basic idea of the numerical scheme is that cubes in the computational domain will be separately mapped to distorted cubes in the physical domain by independent transformations from local coordinates X, Y, Z to Cartesian coordinates x, y, z as illustrated in Figure 1.

The mesh points are the vertices of the mapped cubes, and subscripts i, j, k will be used to denote the value of a quantity at a mesh point. Subscripts $i + \frac{1}{2}, j + \frac{1}{2}, k + \frac{1}{2}$ will be used to denote points mapped from the centers of

the cubes in the computational domain. In developing the difference formulas it will be convenient to introduce averaging the difference operators through the notation

$$\mu_X f = \frac{1}{2}(f_{i+\frac{1}{2},j,k} + f_{i-\frac{1}{2},j,k})$$

$$\delta_X f = f_{i+\frac{1}{2},j,k} - f_{i-\frac{1}{2},j,k}$$

with similar formulas for $\mu_y, \mu_z, \delta_y, \delta_z$. It will also be convenient to use notations such as

$$
\begin{aligned}
\mu_{XX} f &= \mu_X(\mu_X f) \\
&= \frac{1}{4}f_{i+1,j,k} + \frac{1}{2}f_{i,j,k} + \frac{1}{4}f_{i-1,j,k} \\
\mu_{XY} f &= \mu_X(\mu_Y f) \\
\delta_{XX} f &= \delta_X(\delta_X f) \\
&= f_{i+1,j,k} + 2f_{i,j,k} + f_{i-1,j,k} \\
\delta_{XY} f &= \delta_X(\delta_Y f)
\end{aligned}
$$

Numbering the vertices of a particular cube from 1 to 8 as in Figure 1, the local mapping is constructed by a trilinear form in which the local coordinates lie in the range $-\frac{1}{2} \leq X \leq \frac{1}{2}, -\frac{1}{2} \leq Y \leq \frac{1}{2}, -\frac{1}{2} \leq Z \leq \frac{1}{2}$, so the vertices are at $X_i = \pm\frac{1}{2}, Y_i = \pm\frac{1}{2}, Z_i = \pm\frac{1}{2}$. Thus if the Cartesian coordinates of the ith vertex of the mapped cube are x_i, y_i, z_i, the local mapping is defined by

$$x = 8 \sum_{i=1}^{8} x_i \left(\frac{1}{4} + X_i X\right)\left(\frac{1}{4} + Y_i Y\right)\left(\frac{1}{4} + Z_i Z\right) \tag{8}$$

with similar formulas for y, z. The potential Φ is assumed to have a similar form inside the cell:

$$\Phi = 8 \sum_{i=1}^{8} \Phi_i \left(\frac{1}{4} + X_i X\right)\left(\frac{1}{4} + Y_i Y\right)\left(\frac{1}{4} + Z_i Z\right) \tag{9}$$

These formulas preserve the continuity of x, y, z and at the boundary between any pair of cells, because the mappings in each cell reduce to the same bilinear form at the common face. At the center of a computational cell the derivatives of the transformation can be evaluated from equation (8) by formulas such as

$$
\begin{aligned}
x_X &= \frac{1}{4}(x_2 - x_1 + x_4 - x_3 + x_6 - x_5 + x_8 - x_7) \\
&= \mu_{YZ}\, \delta_X\, x
\end{aligned}
$$

Similarly it follows from equation (9) that

$$\Phi_X = \mu_{YZ}\, \delta_X\, \Phi, \qquad \Phi_{XY} = \mu_Z\, \delta_{XY}\, \Phi, \qquad \Phi_{XYZ} = \delta_{XYZ}\, \Phi$$

These formulas are simply an application of the box difference scheme.

Equation (1) will now be represented as a flux balance. For this purpose we introduce a secondary set of cells interlocking with the primary cells as illustrated in Figure 2.

In the computational domain the faces of the secondary cells span the midpoints of the primary cells. Since one secondary cell overlaps eight primary cells, in each of which there is a separate transformation, the secondary cells do not necessarily have smooth faces when they are mapped to the physical domain, but this is not important since their purpose is simply to serve as control volumes for the flux balance.

In order to derive the formula for the flux balance it is convenient to resort to tensor notation. Let the Cartesian and local coordinates be

$$x^1 = x, \quad x^2 = y, \quad x^3 = z$$

$$X^1 = X, \quad X^2 = Y, \quad X^3 = Z$$

The appearance of a repeated index in any formula will be understood to imply a summation over that index. Let H be the transformation matrix with elements $\frac{\partial x^i}{\partial X^j}$ and let h be the determinant of H. Let G be the matrix $H^T H$ with elements

$$g_{ij} = \frac{\partial x^k}{\partial X^i} \frac{\partial x^k}{\partial X^j} \tag{10}$$

Then G is the metric tensor. Also let g^{ij} be the elements of G^{-1}. Then the contravariant velocity components are

$$U = U^1, \quad V = U^2, \quad W = U^3$$

where

$$U^i = g^{ij} \frac{\partial \Phi}{\partial X^j} \tag{11}$$

It may be verified by applying the chain rule for partial derivatives that equation (1) can be written in the local coordinate system as

$$\frac{\partial}{\partial X^i}(\rho h U^i) = 0 \tag{12}$$

This corresponds to a well known formula for the divergence of a contravariant vector. In the computation of the density from equation (4) we now use the formula

$$q^2 = U^i \frac{\partial \Phi}{\partial X^i} \tag{13}$$

Also at a boundary $S(x, y, z) = $ constant, the condition that the normal velocity component is zero becomes

$$U^i \frac{\partial S}{\partial X^i} = 0$$

5

The mesh will be generated so that the boundary will coincide with faces of cells adjacent to the boundary. Thus the boundary condition will reduce to a simple form such as $V = 0$ on a cell face.

The formula for the local flux balance can now be written down by a second application of the box scheme on the secondary cells. Thus equation (12) is approximated by

$$\mu_{YZ} \; \delta_X \; (\rho h U) + \mu_{ZX} \; \delta_Y \; (\rho h V) + \mu_{XY} \; \delta_Z \; (\rho h W) = 0. \qquad (14)$$

The physical interpretation of the quantities $\rho h U, \rho h V, \rho h W$ is that they are the fluxes across the faces of the secondary cell. Consequently this formula is equivalent to calculating the flux across the part of a face of a secondary cell lying in a particular primary cell by using values for ρ, h, U, V, W calculated at the center of that primary cell.

Adjacent to the body the flux balance is established on secondary cells bounded on one or more faces by the body surface as illustrated in Fig 3. There is no flux across these faces and equation (14) is correspondingly modified.

Observe that equation (14) could also be derived from the Bateman variational principle. Suppose that the integral I defined by equation (7) is approximated by summing the volume of each primary cell multiplied by the pressure at its mid-point. Then on setting the derivative of I with respect to each nodal value $\Phi_{i,j,k}$ equal to zero to represent the fact that I is stationary, one recovers equation (14). In a finite element method using isoparametric trilinear elements the contribution of each cell would be calculated by an internal integration over the cell, allowing for the fact that according to the trilinear formulas p is not constant inside the cell.

The use of values of ρ, h, U, V, W calculated at the centers of the primary cells in equation (14), instead of values averaged over the relevant faces, simplifies the formulas at the expense of a "lumping error". Fortunately the contributions to the lumping error from adjacent primary cells offset each other. In fact, if we suppose the vertices of the cells to be generated by a global mapping smooth enough to allow Taylor series expansions of x, y, z as functions of X, Y, Z, then it can be seen from the interpretation of equation (14) as a box scheme that the local discretization error is of second order.

The introduction of lumped quantities in equation (14) is the source, however, of another difficulty. this is most easily seen by considering the case of incompressible flow in Cartesian coordinates. Setting $h = 1, \rho = 1$, equation (14) reduces in the two dimensional case to

$$\mu_{YY}\delta_{XX}\Phi + \mu_{XX}\delta_{YY}\Phi = 0$$

This is simply the rotated Laplacian as illustrated in Figure 4. The odd and even points are decoupled, leading to two independent solutions as sketched. In

fact $\mu_{YY}\delta_{XX}\Phi$ and $\mu_{XX}\delta_{YY}\Phi$ are separately zero for $\Phi = 1$ at odd points, -1 at even points.

To overcome this difficulty, observe that it is due to the evaluation of the flux across the face labeled AB in Figure 5 using a value of calculated at the point A.

If we add a compensation flux $\varepsilon \ \Delta Y \ \Phi_{XY}$ across AB, the point at which Φ_X is effectively evaluated is shifted from A to B as is increased from 0 to 1/2. Taking the cell height ΔY as unity, consistent with the trilinear formula (8), the addition of similar compensation terms on all faces produces the scheme

$$\mu_{YY}\delta_{XX} \ \Phi + \mu_{XX}\delta_{YY} \ \Phi - \varepsilon \ \delta_{XXYY} \ \Phi = 0$$

Notice that setting $\varepsilon = \frac{1}{2}$ yields the standard five point scheme for Laplace's equation, while setting $\varepsilon = \frac{1}{3}$ yields the nine point fourth order accurate scheme.

In order to compensate for the lumping error in equation (14) in a similar manner, we first calculate influence coefficients giving the effective weight of $\delta_{XX}\Phi$, $\delta_{YY}\Phi$, $\delta_{ZZ}\Phi$ in equation (14) when the dependence of ρ on Φ_X, Φ_Y, Φ_Z is accounted for. These are

$$A_X = \rho h \left(g^{11} - \frac{U^2}{a^2} \right)$$

$$A_Y = \rho h \left(g^{22} - \frac{V^2}{a^2} \right)$$

$$A_Z = \rho h \left(g^{33} - \frac{W^2}{a^2} \right) \tag{15}$$

Now define

$$Q_{XY} = (A_X + A_Y) \ \mu_Z \ \delta_{XY} \ \Phi. \tag{16}$$

with similar formulas for Q_{YZ}, Q_{ZX}, and

$$Q_{XYZ} = (A_X + A_Y + A_Z) \ \delta_{XYZ} \ \Phi \tag{17}$$

Then the final compensated equation is

$$\mu_{YZ} \ \delta_X \ (\rho h U) + \mu_{ZX} \ \delta_Y \ (\rho h V) + \mu_{XY} \ \delta_Z \ (\rho h W)$$

$$-\varepsilon \left\{ \mu_Z \ \delta_{XY} \ Q_{XY} + \mu_X \ \delta_{YZ} \ Q_{YZ} + \mu_Y \ \delta_{ZX} \ Q_{ZX} - \frac{1}{2}\delta_{XYZ} \ Q_{XYZ} \right\} = 0 \tag{18}$$

where $0 \leq \varepsilon \leq \frac{1}{2}$. This procedure has proved effective in suppressing high frequency oscillations in the solution.

This completes the definition of the discretization scheme for subsonic flow. It remains to add an artificial viscosity to desymmetrize the scheme in the supersonic zone. Instead of equation (12) we shall satisfy the modified flux balance equation

$$\frac{\partial}{\partial X}(\rho h U + P) \ + \frac{\partial}{\partial Y}(\rho h V + Q) \ + \frac{\partial}{\partial Z}(\rho h W + R) = 0$$

where the added fluxes P, Q and R are proportional to the cell width in the physical domain. Thus the correct conservation law will be recovered in the limit as the cell width decreases to zero. The added terms are designed to produce an upwind bias in the supersonic zone. As in the case of previous schemes for solving the potential flow equation in conservation form[5,6], they are modeled on the artificial viscosity of the nonconservative rotated difference scheme,[4] which has proved reliable in numerous calculations.

First we introduce the switching function

$$\mu = \max \left[0, \left(1 - \frac{a^2}{q^2} \right) \right]$$

Then P, Q, R are constructed to that

$$P \;\; approximates \;\; -\mu \, |U| \, \delta_X \, \rho$$
$$Q \;\; approximates \;\; -\mu \, |V| \, \delta_Y \, \rho$$
$$R \;\; approximates \;\; -\mu \, |W| \, \delta_Z \, \rho$$

with an upwind shift in each case. Since $\mu = 0$ when $q < a$, the added terms vanish in the subsonic zone. In the numerical scheme equation (18) is actually modified by the addition of the terms

$$\delta_X P \; + \; \delta_Y Q \; + \; \delta_Z R$$

In order to form P, Q, R we first construct

$$\hat{P} = \mu h \frac{\rho}{a^2} \left(U^2 \, \delta_{XX} + UV \, \mu_{XY} \, \delta_{XY} + WU \, \mu_{ZX} \, \delta_{ZX} \right) \Phi$$

$$\hat{Q} = \mu h \frac{\rho}{a^2} \left(UV \, \mu_{XY} \, \delta_{XY} + V^2 \, \delta_{YY} + VW \, \mu_{YZ} \, \delta_{YZ} \right) \Phi$$

$$\hat{R} = \mu h \frac{\rho}{a^2} \left(WU \, \mu_{ZX} \, \delta_{ZX} + VW \, \mu_{YZ} \, \delta_{YZ} + W^2 \, \delta_{ZZ} \right) \Phi$$

Then

$$P_{i+\frac{1}{2},j,k} = \begin{cases} \hat{P}_{i,j,k} & \text{if } U > 0 \\ \hat{P}_{i+1,j,k} & \text{if } U < 0 \end{cases}$$

with similar shifts for Q, R.

The motivation for these formulas is provided by the following analysis. When equation (12) is represented explicitly in quasilinear form, its leading terms are

$$\frac{\rho h}{a^2} \left\{ (a^2 - q^2)\Phi_{ss} \; + \; a^2(\Delta\Phi - \Phi_{ss}) \right\} = 0$$

where s is the local flow direction, and Δ is the Laplacian. In the transformed coordinate system

$$\frac{\partial \Phi}{\partial s} = \frac{U^i}{q} \frac{\partial \Phi}{\partial X^i}$$

so the leading terms of Φ_{ss} are $\frac{U^i U^j}{q^2} \frac{\partial^2 \Phi}{\partial X^i \partial X^j}$. According to the rotated difference scheme one should use upwind difference formulas to evaluate Φ_{ss} at supersonic points, as illustrated in Figure 6. Now the upwind formula for Φ_{XX} can be regarded as an approximation to $\Phi_{XX} - \Delta X \Phi_{XXX}$. Similarly the upwind formula for Φ_{XY} yields an added term $\frac{1}{2} \Delta X \; \Phi_{XXY} \; + \; \frac{1}{2} \Delta Y \; \Phi_{XYY}$ and so on. The use of these formulas in the evaluation of $\frac{\rho h}{a^2}(a^2 - q^2)\Phi_{ss}$ thus produces an effective artificial viscosity

$$-\frac{\rho h}{a^2}\left(1 - \frac{a^2}{q^2}\right)\left\{\Delta X \; U \left(U \; \Phi_{XXX} + V \; \Phi_{YXX} + W \; \Phi_{ZXX}\right)\right.$$

$$+ \Delta Y \; V \left(U \; \Phi_{XYY} + V \; \Phi_{YYY} + W \; \Phi_{ZYY}\right)$$

$$\left. + \Delta Z \; W \left(U \; \Phi_{XZZ} + V \; \Phi_{YZZ} + W \; \Phi_{ZZZ}\right)\right\}$$

assuming that U, V, W are positive. Since $\frac{\partial \rho}{\partial(q^2)} = -\frac{\rho}{2a^2}$ it follows from equation (13) that

$$\rho_X = -\frac{\rho h}{a^2}\left(U\Phi_{XX} + V\Phi_{XY} + W\Phi_{XZ}\right)$$

Thus on setting $\Delta X = 1$, consistent with equation (8), leading terms of $-\left(\frac{\partial}{\partial x}\right)\left(\mu \; U \; \delta_X \; \rho\right)$ are

$$-\frac{\rho h}{a^2}\left(1 - \frac{a^2}{q^2}\right)\Delta X\left(U\Phi_{XXX} + V\Phi_{YXX} + W\Phi_{ZXX}\right)$$

which can be seen to be the desired quantity. Note that the construction of the artificial viscosity is based on the presumption of a smooth mesh in the supersonic zone.

Finally it remains to devise an iterative procedure for solving the nonlinear algebraic equations which result from the discretization. Following the same reasoning as was used for the iterative solution of the rotated difference scheme and earlier schemes in conservation form,[4-6] this is accomplished by embedding the steady state equation in an artificial time dependent equation. Thus we solve a discrete approximation to

$$\frac{\partial}{\partial X}(\rho h U + P) \; + \frac{\partial}{\partial Y}(\rho h V + Q) \; + \frac{\partial}{\partial Z}(\rho h W + R)$$

$$= \alpha\Phi_{XT} \; + \beta\Phi_{YT} \; + \gamma\Phi_{ZT} \; + \delta\Phi_{T}$$

where the coefficients α, β, γ are chosen to make the flow direction timelike, as in the steady state, and controls the damping.

The complete numerical scheme thus calls for the following steps:

1. Calculate the contravariant velocity components and the density in each primary cell using the box scheme.

2. Calculate the flux balance on each secondary cell by a second application of the box scheme.

3. Add compensation terms to offset the effect of lumping errors.

4. Add artificial viscosity at points where the flow is locally supersonic to desymmetrize the scheme and enforce the entropy condition.

5. Add time dependent terms to embed the steady state equation in a convergent time dependent process which evolves to the solution.

4   Results

The finite volume scheme has been used in a number of calculations for swept wings and wing-cylinder combinations, and some results of these calculations are included in this section.[1] The scheme must be provided with the Cartesian coordinates of each mesh point. The meshes for our calculations have been generated by sequences of global mappings. This has the advantage of producing a smooth distribution of mesh points. In contrast with earlier methods in which the equation of motion was explicitly transformed, 4-6 these mappings are now used only to calculate the coordinates of the mesh points.

The following procedure has been used to generate the mesh for a swept wing. First we introduce parabolic coordinates in planes containing the wing section by the transformation

$$\bar{X} + i\bar{Y} = \left\{ \frac{\{x - x_0(z) + i(y - y_0(z))\}}{t(z)} \right\}^{\frac{1}{2}}$$

$$\bar{Z} = z$$

where z is the spanwise coordinate, $x_0(z)$ and $y_0(z)$ define a singular line located just inside the leading edge, and $t(z)$ is a scaling factor which can be adjusted so that the wing chord is covered by the same number of cells at every span station. The effect of this transformation is to unwrap the wing to form a shallow bump

$$\bar{Y} = S(\bar{X}, \bar{Z})$$

as illustrated in Figure 7. Then we use a shearing transformation

$$X = \bar{X}, \qquad Y = \bar{Y} - S(\bar{X}, \bar{Z}), \qquad Z = \bar{Z}$$

to map the wing surface to the plane $Y = 0$. We now lay down a rectangular coordinate system in the X, Y, Z space, and finally generate the volume elements by the reverse sequence of transformations from X, Y, Z to x, y, z. The vortex

sheet trailing behind the wing is assumed to coincide with the cut generated by the sheared parabolic coordinate system.

The mesh for the wing-cylinder calculations has been generated by a simple extension of this procedure, in which the cylinder is mapped to a vertical slit by a preliminary Joukowsky transformation, as sketched in Figure 8. With the fuselage thus compressed into the symmetry plane, we then use the same sequence of mappings as for a swept wing on a wall. The use of a vertical slit rather than a horizontal slit, as was used by Newman and Klunker for small disturbance calculations,[12] allows the wing to be shifted vertically so that both low and high wing configurations can be treated.

Figure 9 shows the result of a calculation for the ONERA M6 wing, for which experimental data is available.[13] The calculation was performed on a sequence of meshes. After the calculation on each of the first two meshes, the number of intervals was doubled in each coordinate direction, and the interpolated result was used as the starting point for the calculation on the next mesh. The fine mesh contained 160 intervals in the chordwise x direction, 16 intervals in the normal y direction, and 32 intervals in the spanwise z direction, for a totally of 81920 cells. 100 relaxation cycles were used on each mesh. Such a calculation requires about 90 minutes on a CDC 6600 or 20 minutes on a CDC 7600. Separate pressure distributions are shown for stations at 20, 45, 65 and 95 percent of the semi-span. The pressure coefficient at which the speed is locally sonic is marked by a horizontal line on the pressure axis, and the experimental data is overplotted on the numerical result, using circles for the upper surface and squares for the lower surface. The calculation did not include a boundary layer correction. It can be seen, however, that the triangular shock pattern is quite well captured, and that the calculated pressure distribution is a fair simulation of the experimental result. The result of this calculation is also in quite good agreement with the result of a previous calculation using the nonconservative rotated difference scheme.[14]

Figure 10 shows the result for the same wing mounted on a low and position on a cylinder. The configuration is scaled so that the radius of the cylinder is 0.25, while the wing tip station is 1.25. No experimental data is available in this case. The calculation shows an increase of lift, particularly near the wing root. This is to be expected, because the cylinder is set at the same angle of attack as the wing and will generate an upwash. The problem of computing the flow past a wing-fuselage combination is discussed at greater length in a companion paper,[15] in which an alternative mesh generating scheme is proposed.

5   Conclusion

The results displayed in Figures 9 and 10 serve to indicate the promise of the finite volume scheme. Its main advantage is the relative ease with which it can

be adapted to treat a variety of complex configurations. Since the treatment of interior points is independent of the particular mappings used to generate the mesh, topologically similar configurations can be treated by the same flow computation routine, provided that suitable mappings can be found to map them to the same computational domain.

This flexibility is achieved at the expense of an increase in the amount of time required for the computations, unless a very large memory capacity is available, because of the need to perform a numerical inversion o the transformation matrix defining the local mapping in each cell. If the inverse transformation coefficients are not saved they must be recalculated at every cycle. In this form the scheme requires about 50 percent more time than the rotated difference scheme to treat a swept wing on an equal number of mesh points. It is worth noting that the computing time could be substantially reduced by restricting the use of distorted cells to an inner region surrounding the body, with a transition to Cartesian coordinates in the outer region.

References

[1] Murman, E.M. and Cole, J.D., Calculation of plane steady transonic flows, AIAA Jour., Vol. 9, 1971, pp. 114-121.

[2] Murman, E.M., Analysis of embedded shock waves calculated by relaxation methods, Proceedings of AIAA Conf. on Computational Fluid Dynamics, Palm Springs, July 1973, pp. 27-40.

[3] Bailey, F.R. and Ballhaus, W.F., Relxation methods for transonic flows about wing-cylinder combinations and lifting swept wings, Proceedings of Third International Conference on Numerical Methods in Fluid Dynamics, Paris, July 1972, Lecture Notes in Physics, Vol. 19, Springer Verlag, 1973, pp.2-9.

[4] Jameson, Antony, Iterative solution of transonic flows over airfoils and wings, including flows at Mach 1, Comm. Pure Appl. Math., Vol. 27, 1974, pp. 283-309.

[5] Jameson, Antony, Numerical solution of nonlinear partial differential equations of mixed type, Numerical Solution of Partial Differential Equations III, SYNSPADE 1975, Academic Press, 1976, pp. 275-320.

[6] Jameson, Antony, Numerical computation of transonic flows with shock waves, Symposium Transsonicum II, Gottingen, September 1975, Springer Verlag, 1976, pp. 384-414.

[7] MacCormack, R.W., Rizzi, A.W. and Inouye, M., Steady supersonic flow fields with embedded subsonic regions, Proceedings of Conference on Computational Problems and Methods in Aero and Fluid Dynamics, Manchester, 1974.

[8] Rizzi, Arthur, Transonic solutions of the Euler equations by the finite volume method, Symposium Transsonicum II, Gottingen, September 1975, Springer Verlag, 1976, pp. 567-574.

[9] Bateman, H., Notes on a differential equation which occurs in the two dimensional motion of a compressible fluid and the associated variational problem, Proc. Roy. Soc. Series A, Vol. 125, 1929, pp. 598-618.

[10] Lax, Peter and Wndroff, Burton, Systems of conservatiokn laws, Comm. Pure Appl. Math., Vol. 13, 1960, pp. 217-237.

[11] Synge, J.L., and Schild, A., Tensor Calculus, Unviersity of Toronto Press, 1949, pp. 57-58.

[12] Newman, Perry A. and Klunker, E.B., Numerical modeling of tunnel wall and body shape effects on transonic flow over finite lifting wings, Aerodynamic Analyses Requiring Advanced Computers, Part 2, NASA, SP-347, 1975, pp. 1189-1212.

[13] Monnerie, B., and Charpin, F., Essais de buffeting d'une aile en fleche en trnassonique, 10^e Colloque d'Aerody-namique Appliquee, Lille, November 1973.

[14] Jameson, Antony and Caughey, D.A., Numerical calculation of the transonic flow past a swept wing, New York University ERDA Report COO 3077-140, May 1977.

[15] Caughey, D.A. and Jameson, Antony, Numerical calculation of transonic potential flow about wing-fuselage combiantions, AIAA Paper 77-677, June 1977.

ONERA
MACH
Z

x,y,z   X,Y,Z

Figure 1

x,y,z   X,Y,Z

Figure 2

x,y,z   X,Y,Z
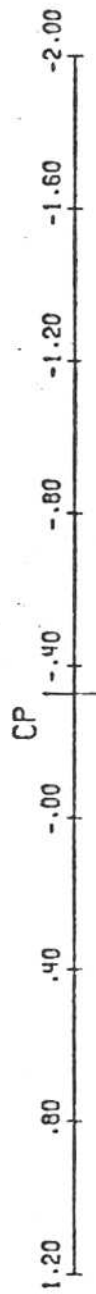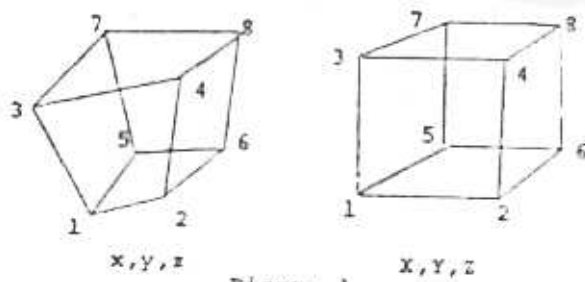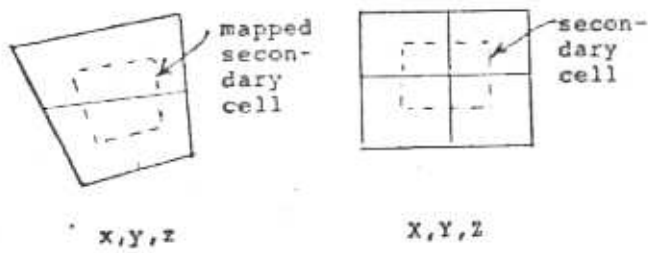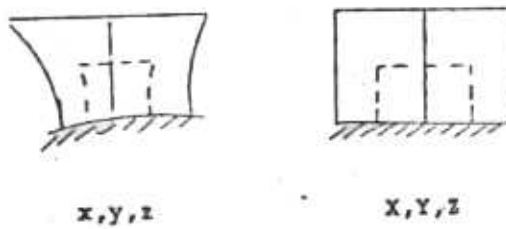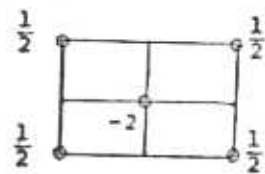
Figure 3

(a) Stencil of rotated Laplacian.   (b) Decoupled solution at odd and even points.
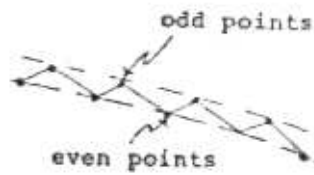
Figure 4

shift evaluation of
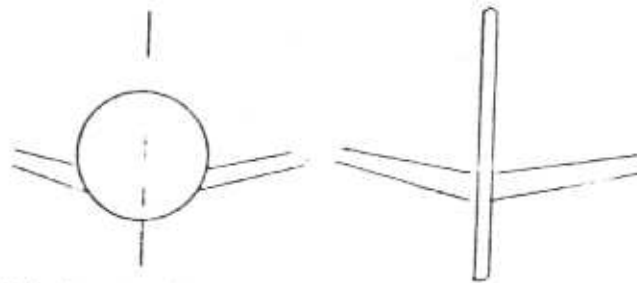ϕ_X up by adding
$\epsilon \Delta Y \phi_{XY}$

Figure 5

velocity

Figure 6

singular line

B   C
            A

x,y,z

A   B   C

singular line

$\bar{x}, \bar{y}, \bar{z}$
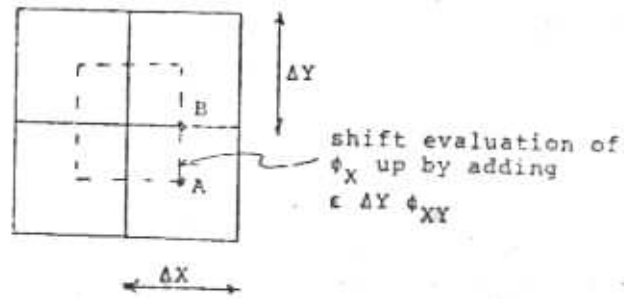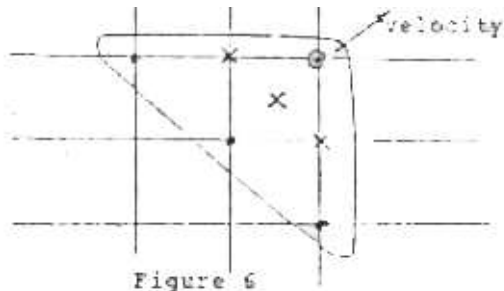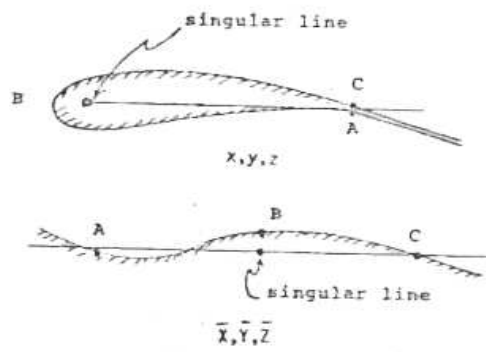
Figure 7

(a) Front view of
wing-cylinder
combination.

(b) Cylinder mapped
to a vertical
slit.

Figure 8
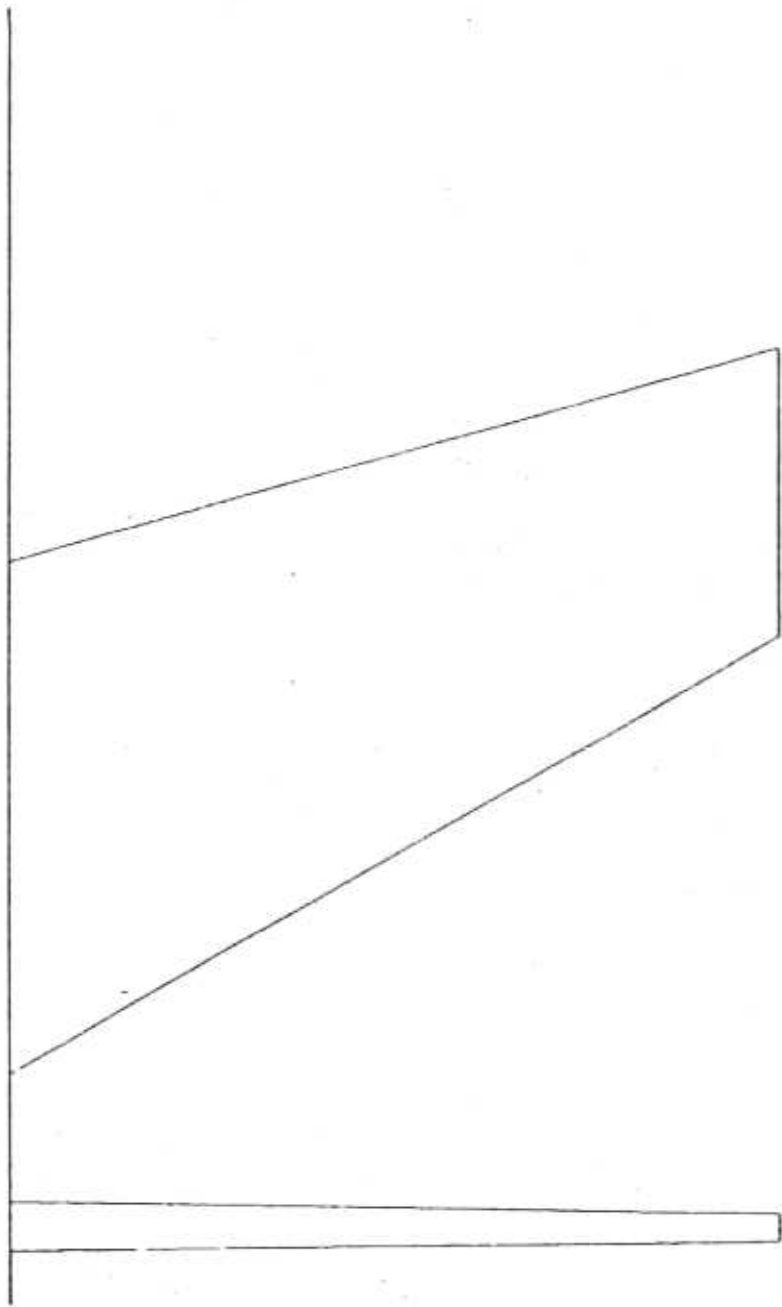
ONERA WING M6

FIGURE 9(A)
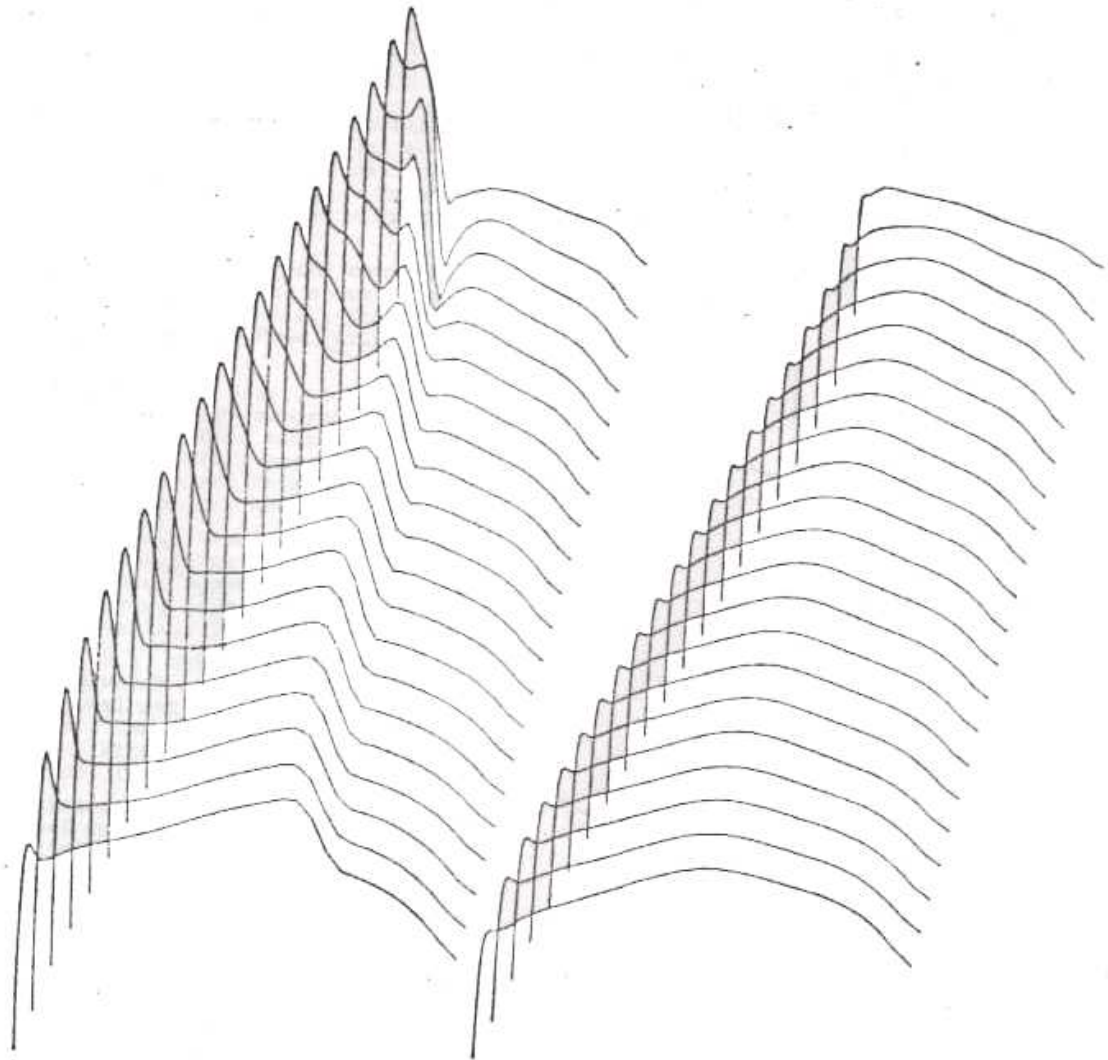
UPPER SURFACE PRESSURE   LOWER SURFACE PRESSURE

ONERA WING M6
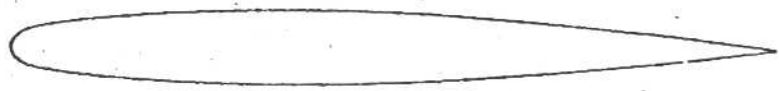MACH   .840   YAW   0.000   ALPHA   3.060

FIGURE 9(B)
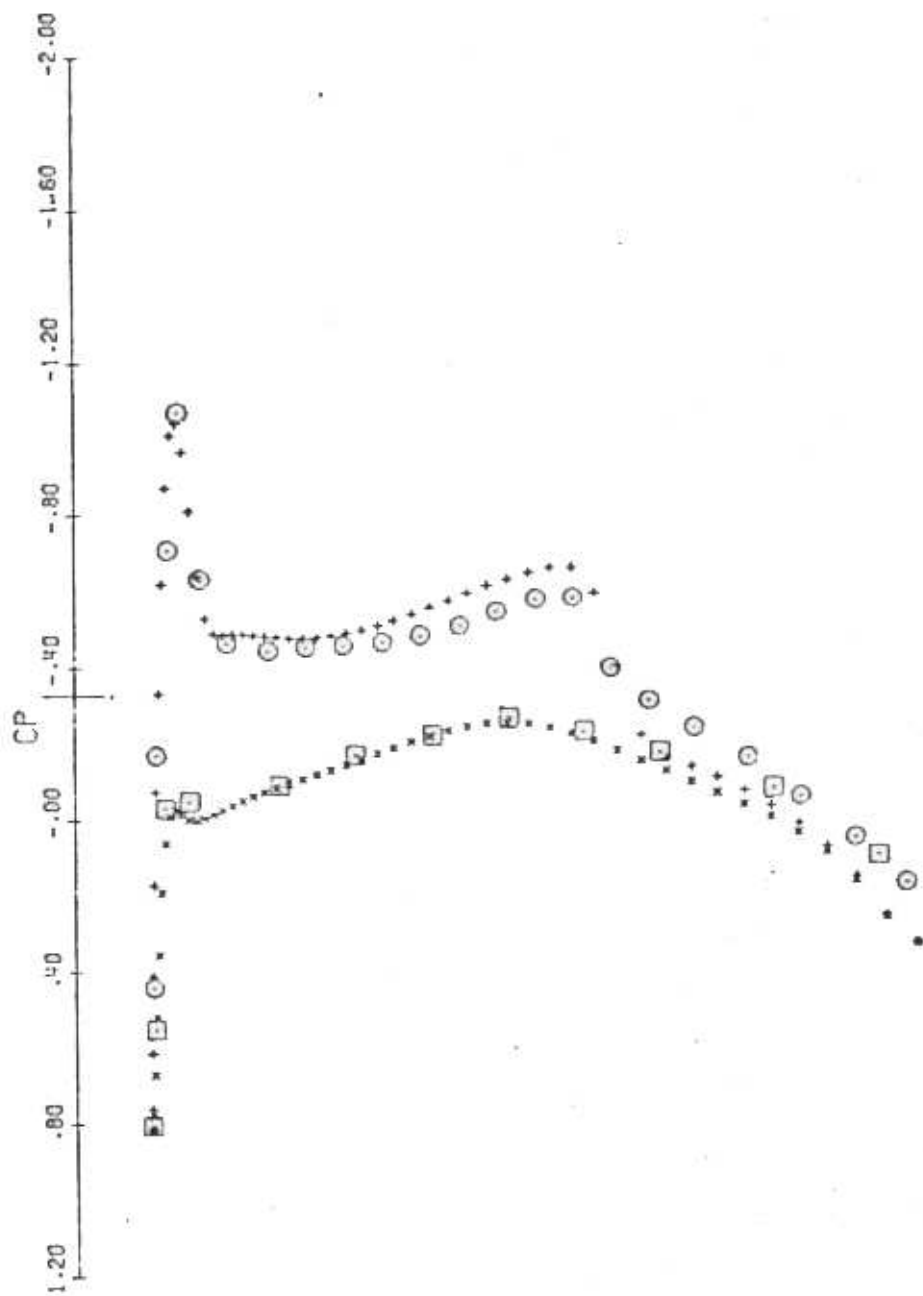
ONERA WING M6
MACH	.840	YAW	0.000	ALPHA	3.060
Z	.20	CL	.2733	CD	.0151

FIGURE 9(C)

+, x   THEORY
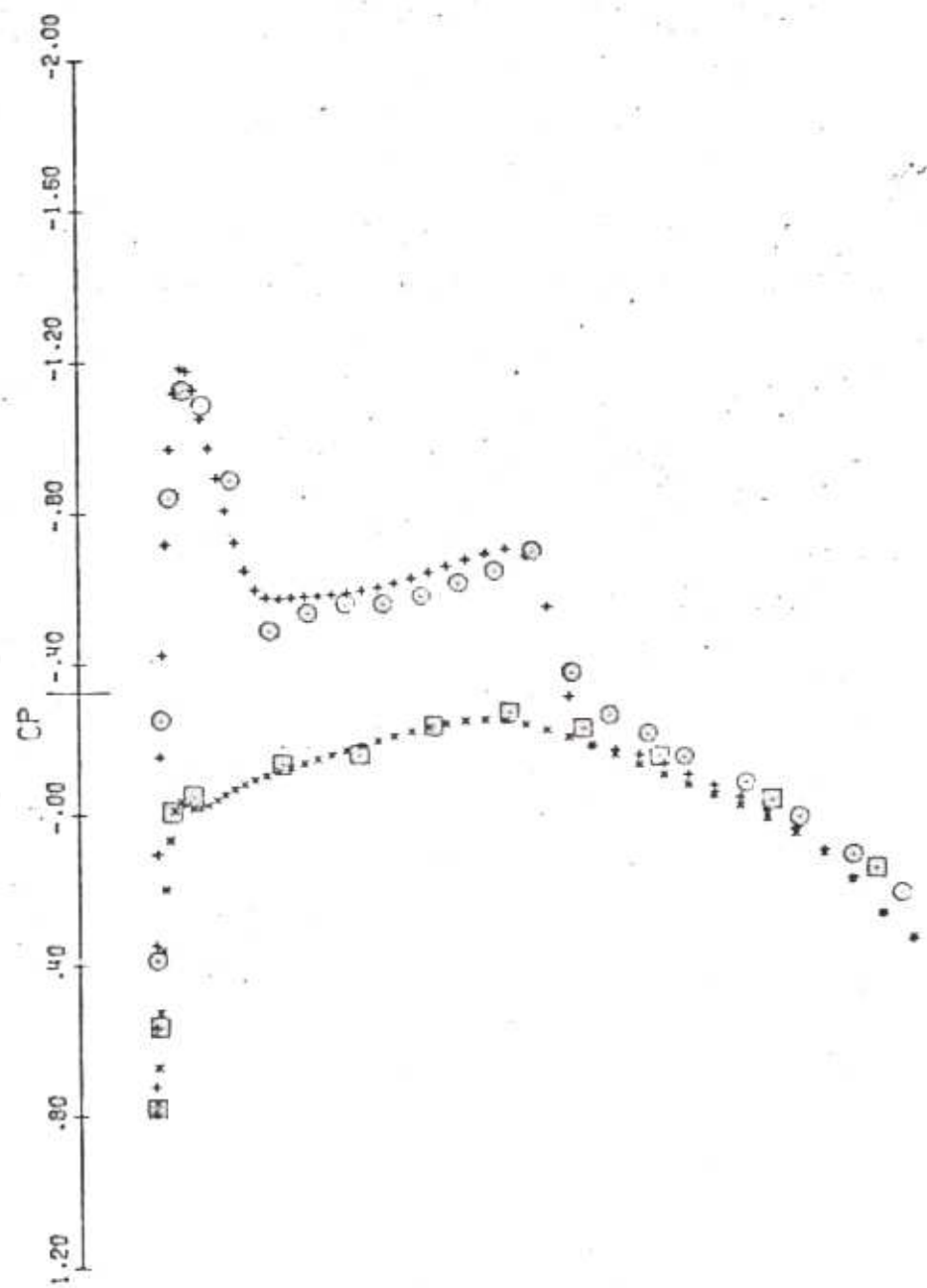
⊙, ⊡   EXPERIMENT

ONERA WING M6

| MACH | .840 | YAW | 0.000 | ALPHA | 3.060 |
| Z | .45 | CL | .2942 | CD | .0051 |

FIGURE 9(D)
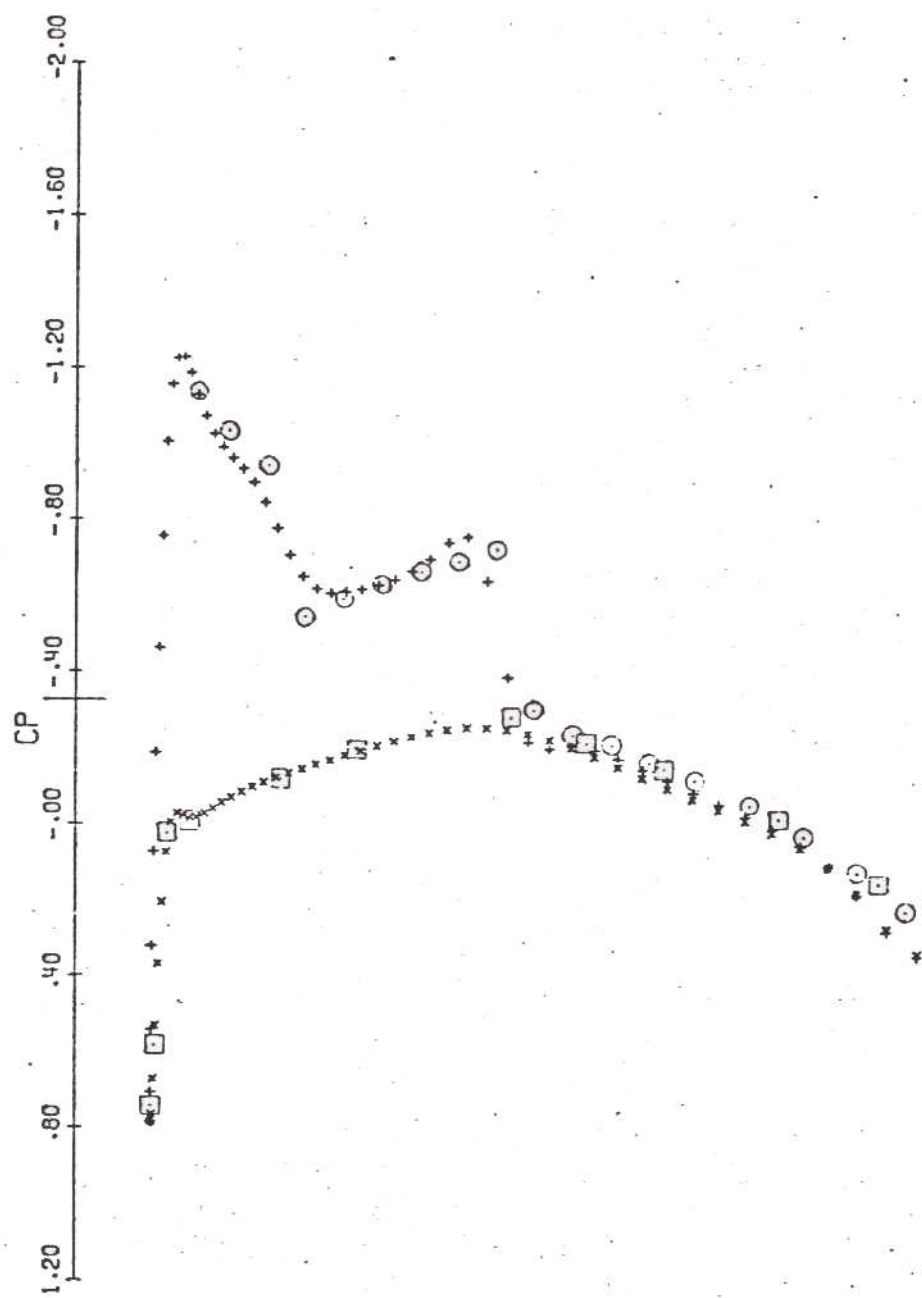
+, × THEORY

⊙, ⊡ EXPERIMENT

ONERA WING M6
MACH   .840   YAW   0.000   ALPHA 3.060
Z   .65   CL   .2936   CD   -.0006
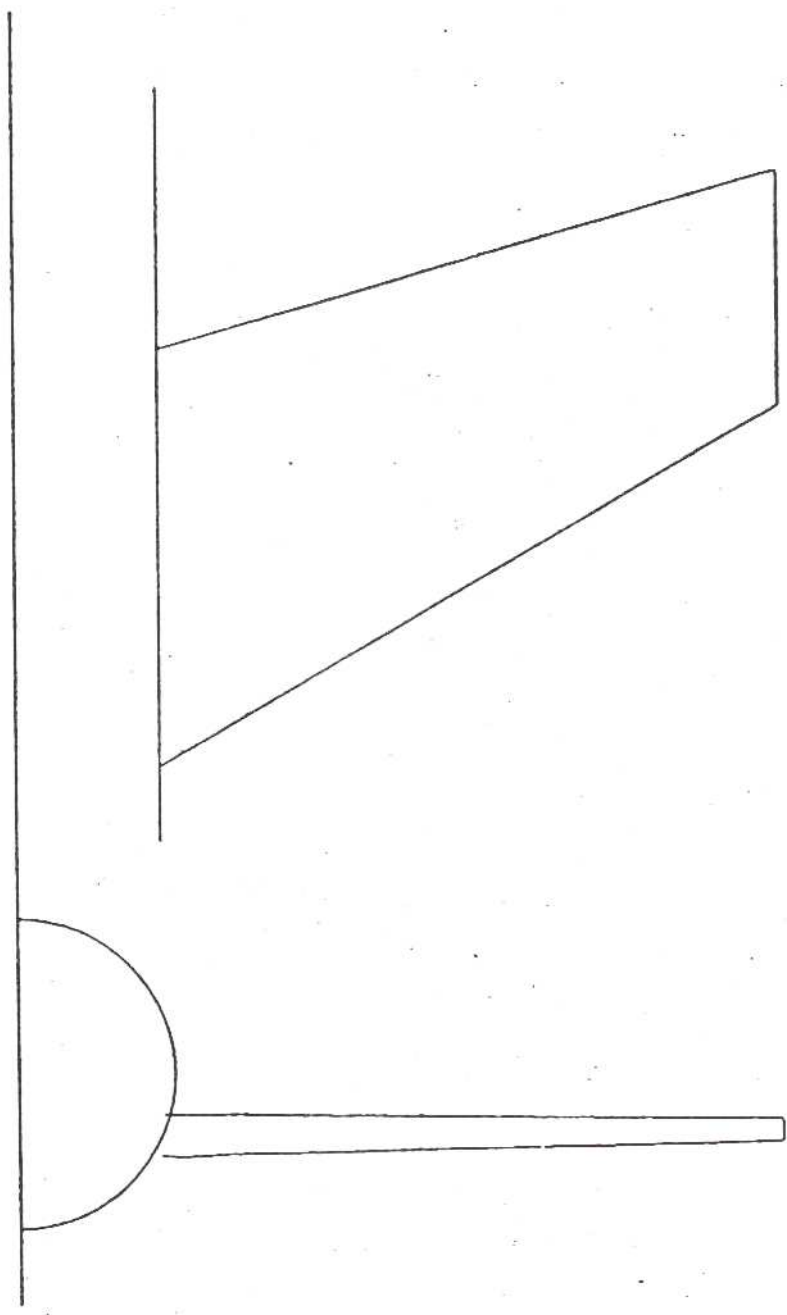
FIGURE 9(E)

+, x   THEORY
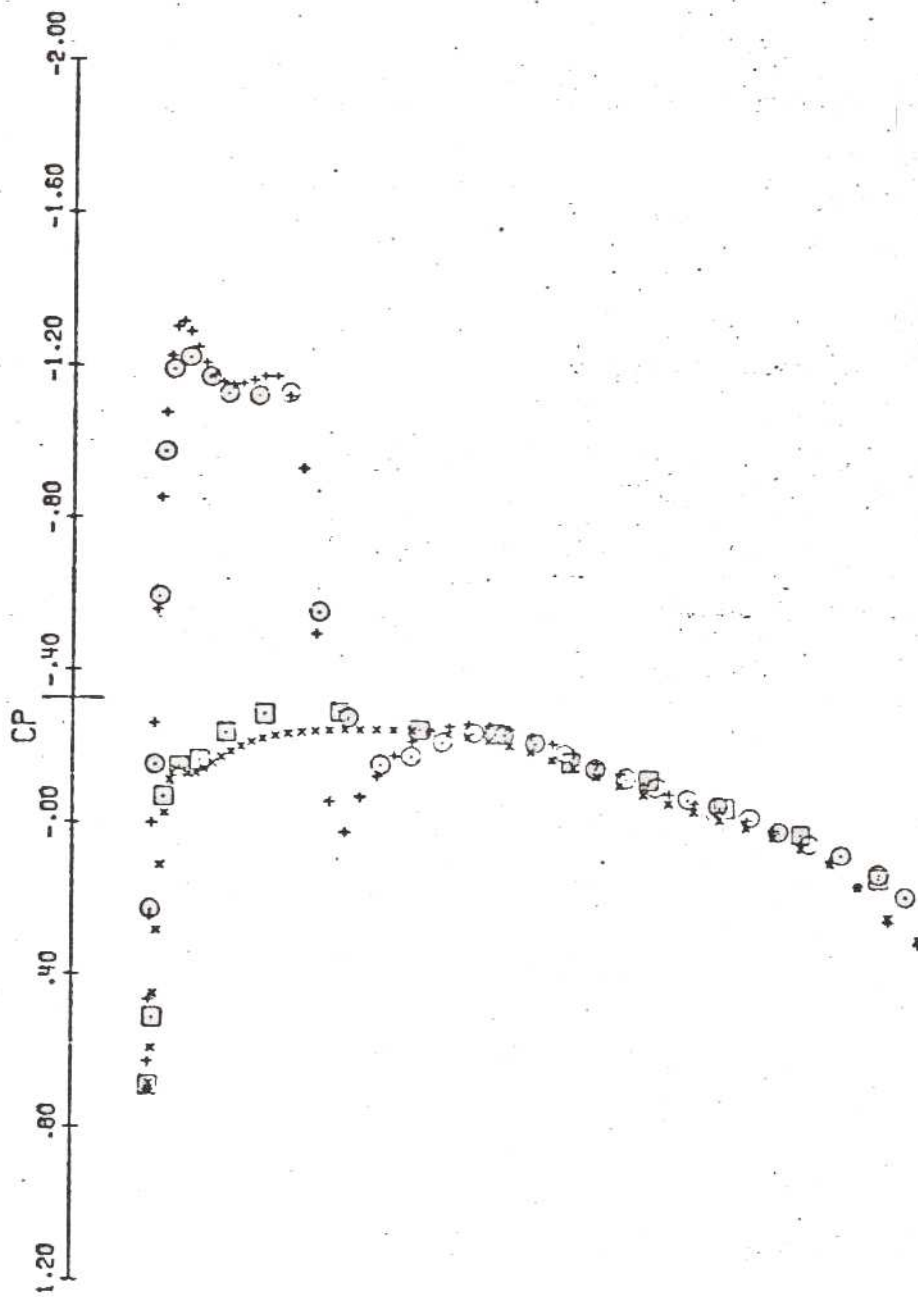
⊙, ▣   EXPERIMENT

CNERA WING M6
MACH   .840   YAW   0.000   ALPHA 3.060
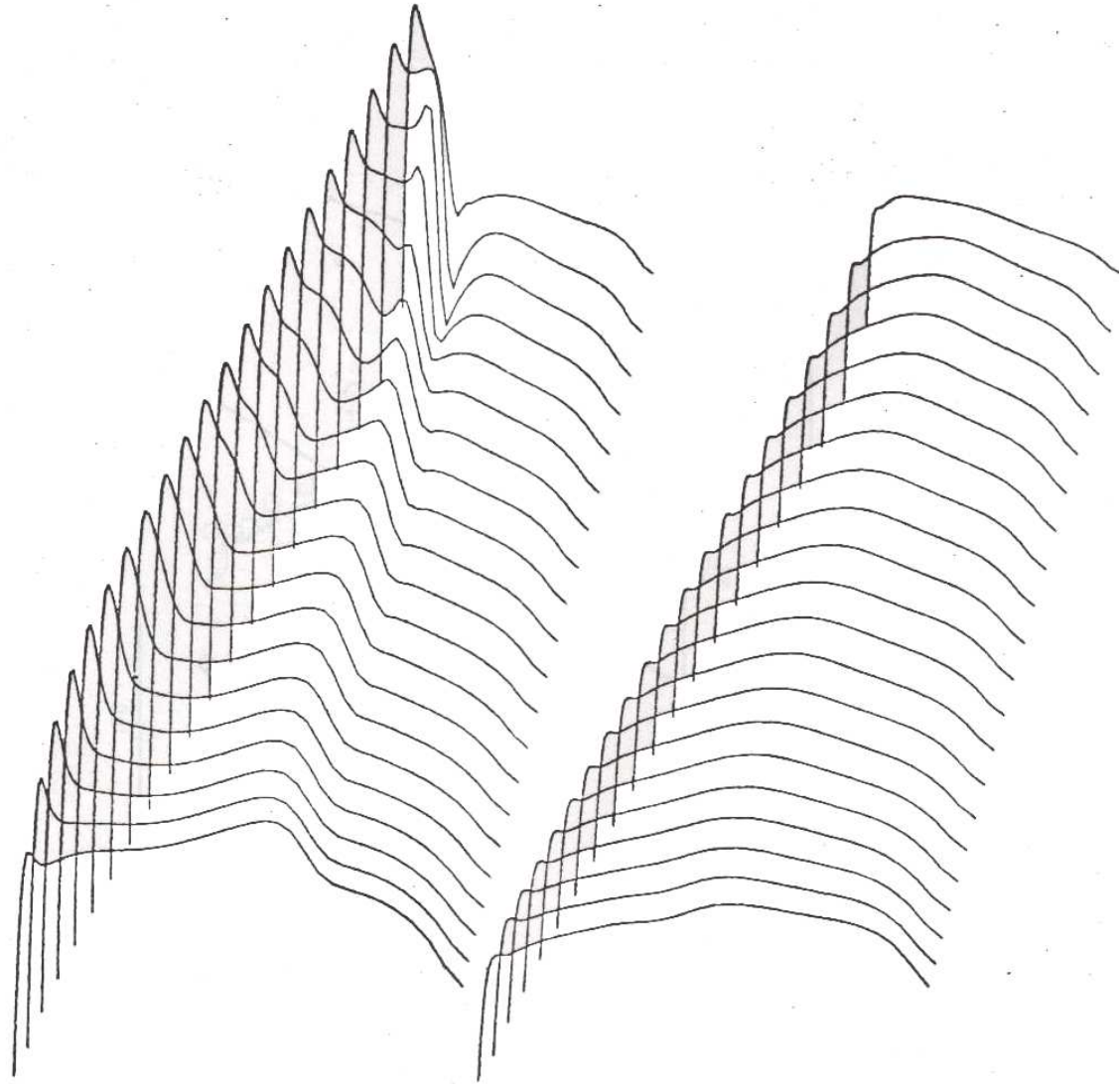Z   .95   CL   .2004   CD   -.0146

FIGURE 9(F)

+, x   THEORY
O, □   EXPERIMENT

ONERA WING M6

FIGURE 10(A)

UPPER SURFACE PRESSURE   LOWER SURFACE PRESSURE
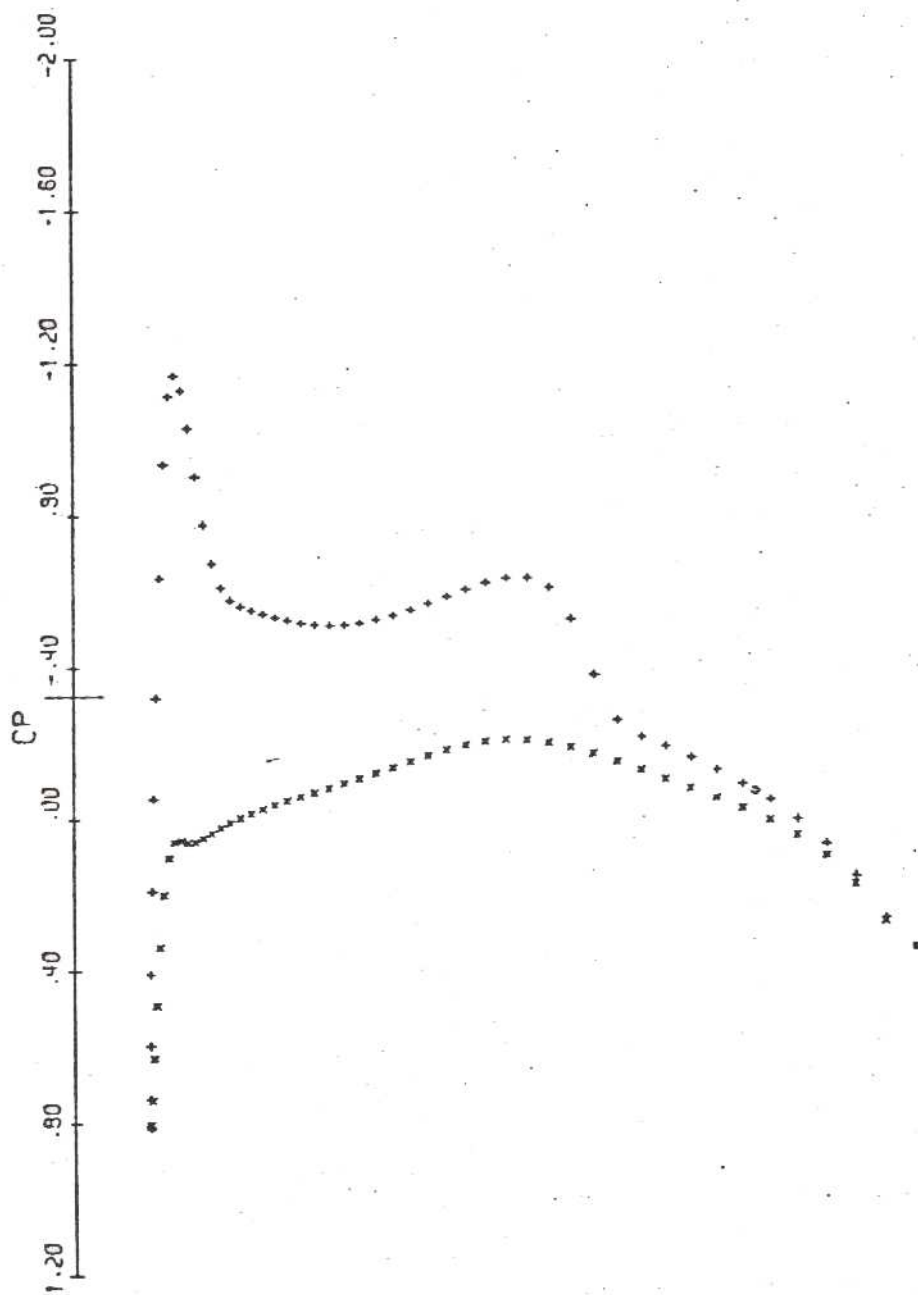
ONERA WING M6
MACH   .840   YAW   0.000   ALPHA   3.060

FIGURE 10(B)

ONERA WING M6

MACH   .840   YAW   0.000   ALPHA   3.060
Z   .43   CL   .3216   CD   .0147

FIGURE 10(C)

ONERA WING M6

MACH	.840	YAW	0.000	ALPHA	3.060
Z	.68	CL	.3357	CD	.0055

FIGURE 10(D)